Materials Research Letters

ISSN: (Print) 2166-3831 (Online) Journal homepage: http://www.tandfonline.com/loi/tmrl20

Mesoporous MXene powders synthesized by acid induced crumpling and their use as Na-ion battery anodes

Varun Natu, Mallory Clites, Ekaterina Pomerantseva & Michel W. Barsoum

To cite this article: Varun Natu, Mallory Clites, Ekaterina Pomerantseva & Michel W. Barsoum (2018) Mesoporous MXene powders synthesized by acid induced crumpling and their use as Na-ion battery anodes, Materials Research Letters, 6:4, 230-235, DOI: 10.1080/21663831.2018.1434249

To link to this article: https://doi.org/10.1080/21663831.2018.1434249

MATER. RES. LETT., 2018
VOL. 6, NO. 4, 230–235
https://doi.org/10.1080/21663831.2018.1434249

MATERIALS RESEARCH LETTERS
Taylor & Francis
Taylor & Francis Group

ORIGINAL REPORT

Mesoporous MXene powders synthesized by acid induced crumpling and their use as Na-ion battery anodes

Varun Natu, Mallory Clites, Ekaterina Pomerantseva and Michel W. Barsoum

Department of Materials Science and Engineering, Drexel University, Philadelphia, PA, USA

ABSTRACT

Manipulating the shapes of, otherwise flat, two-dimensional, 2D, flakes is important in many applications. Herein by simply decreasing the pH of a $Ti_3C_2T_x$ MXene colloidal suspension, the 2D nanolayers crash out into crumpled flakes, resulting in randomly oriented powders, with a mesoporous architecture. Electrodes made with the latter showed capacities of 250 mAh g^{-1} at 20 mA g^{-1} in sodium-ion batteries. The rate performance, 120 mAh g^{-1} at 500 mA g^{-1}, was also respectable. This acid-induced, reversible, crumpling approach is facile and scalable and could prove important in electrochemical, biological, catalytic, and environmental MXene-based applications.

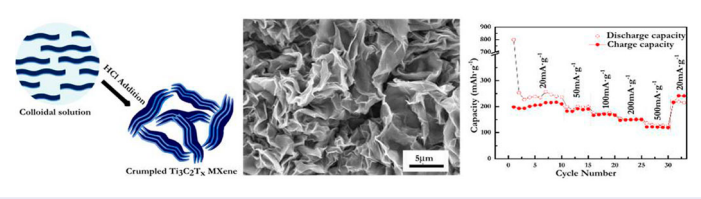

IMPACT STATEMENT

By simply decreasing the pH of a $Ti_3C_2T_x$ colloidal suspension, we induce the 2D flakes flocculate into mesoporous crumpled flakes, that we then show can be used as Na-ion battery anodes.

ARTICLE HISTORY
Received 2 November 2017

KEYWORDS
MXenes; crumpled nanosheets; acid-induced crashing; 3D mesoporous architecture; sodium-ion battery

Introduction

Two-dimensional, 2D, transition metal carbides and nitrides, known as MXenes [1,2], have gained a lot of interest lately due to their high carrier densities resulting in metal-like conductivities combined with hydrophilicity. Their potential has already been proven in a range of applications including energy storage [3], water purification [4], hydrogen storage [5], photovoltaics [6], and electromagnetic interference shielding [7], among many others. The MXenes moniker is derived from their parent layered MAX phases. The latter have a chemical formula of $M_{n+1}AX_n$, where M is an early transition metal, A is an element mostly from group 13 or 14, and X can be C and/or N [8,9]. MXenes are mostly synthesized by etching of the A layer from the MAX phases using hydrofluoric acid, HF, or lithium fluoride salts, such as LiF, and hydrochloric acid, HCl. When the A layers are etched, the surface of the resulting 2D layers is functionalized with various terminations, T. Therefore, the actual chemistry of MXenes is usually described by the formula $M_{n+1}X_nT_x$, where T is a combination of −O, −OH, and −F surface terminations.

Computational studies have predicted capacities between 217 and 351 mAh g^{-1}, depending on the type of surface terminations, when $Ti_3C_2T_x$ is used as an anode in Na-ion electrochemical cells [10–12]. Experimentally, electrodes made with etched, but non-delaminated, $Ti_3C_2T_x$ flakes, also referred to herein as multilayers, MLs, exhibited a capacity of 100 mAh g^{-1}. This capacity almost vanishes when electrodes of the same composition were prepared using vacuum filtration of delaminated nanosheets due to the dense packing of the 2D nanoparticles. resulting in poor electrolyte penetration [13,14].

Several strategies have been attempted to overcome this problem. Xie et al. used carbon nanotubes (CNTs)

CONTACT Michel W. Barsoum barsoumw@drexel.edu Department of Materials Science and Engineering, Drexel University, Philadelphia, PA 19104, USA

Supplemental data for this article can be accessed here. https://doi.org/10.1080/21663831.2018.1434249

as spacers in vacuum filtered $Ti_3C_2T_x$ MXene films to facilitate electrolyte penetration, which led to a nearly fivefold increase in capacity compared to those of MXene films without CNTs [14]. Zhao et al. fabricated $Ti_3C_2T_x$ films with poly(methyl methacrylate) templating spheres. When the spheres were subsequently burned out, $Ti_3C_2T_x$ films, with large hollow pores, were created. These electrodes showed an initial capacity of 370 mAh g^{-1}at 0.25 C [15]. Even though this is the highest capacity value reported for $Ti_3C_2T_x$ in Na-ion cells, the synthesis procedure is complex, not easily scalable and the resulting electrodes are fragile. Lian et al. showed that simple shaking of the etched MXene ML particles in KOH resulted in their delamination and formation of $Ti_3C_2T_x$ nanoribbons which exhibited a capacity of 150 mAh g^{-1} at a current density of 20 mA g^{-1} [16]. However, these electrodes do not perform well at current densities above 200 mA g^{-1} and show nearly the same capacities as those of just etched MXenes at higher currents in Na-ion batteries. Therefore, new facile and cost-effective methods need to be developed for creating high capacity, porous MXene electrodes with good ion accessibility to the electrolyte.

As far as we are aware the only three reports in which $Ti_3C_2T_x$ flakes were crumpled, used processes such as spray drying [17], Calixarene directed synthesis [18], and freeze drying [19]. The main goal of this work is to describe a facile method for crumpling MXene flakes. To demonstrate that this crumpling can enhance properties, we used the crumpled powders as Na-ion electrodes and showed that they performed better than their multilayered, ML, counterparts. No attempts were made to optimize the electrode architecture. Nonetheless, the results obtained, as shown below, were surprisingly good. Herein, we employ a simple, purely chemical approach. We show that by simply reducing the pH of a $Ti_3C_2T_x$ colloidal suspension, using common acids such as hydrochloric acid, HCl, the individual MXene nanosheets crumple and readily flocculate resulting in a foam-like, 3D, mesoporous open architecture with a more random orientation of the nanosheets, than if they had been filtered. These powders will henceforth be referred to as crumpled, or *c*-$Ti_3C_2T_x$. For reasons that are discussed below, we also fabricated filtered films, which will henceforth be referred to as *f*-$Ti_3C_2T_x$. Figure 1 shows a schematic of how the *c*-$Ti_3C_2T_x$ powders and filtered films are obtained. The experimental and electrochemical testing procedure details can be found in Supporting Information.

X-Ray diffraction (XRD) patterns of Ti_3AlC_2, *c*-$Ti_3C_2T_x$, and *f*-$Ti_3C_2T_x$ (Figure 2) confirm that the MAX phase was fully converted to MXene. Furthermore, the

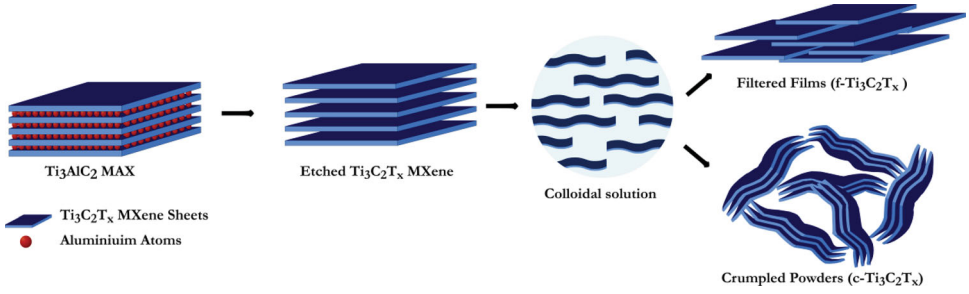

Figure 1. Schematic illustration of the synthesis process producing crumpled MXene nanosheets or filtered films. The latter are made by filtering a colloidal suspension.

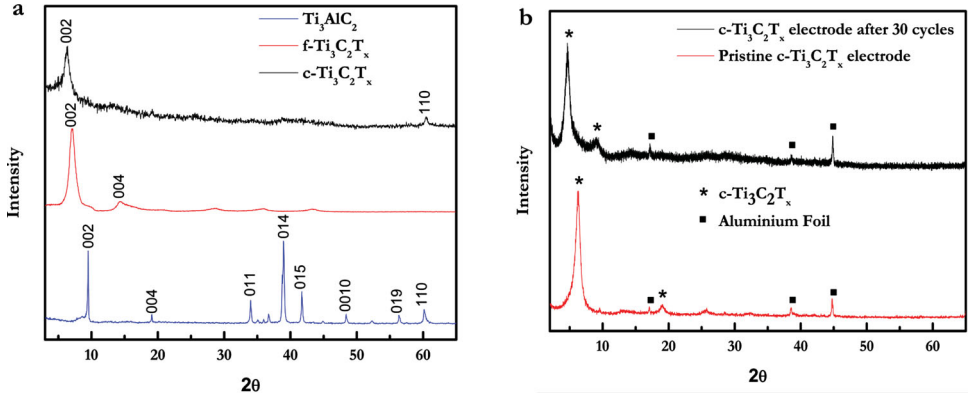

Figure 2. XRD patterns of (a) *c*-$Ti_3C_2T_x$ (top, black), *f*-$Ti_3C_2T_x$ (center, red) and parent Ti_3AlC_2 MAX (bottom, blue) powders; (b) pristine *c*-$Ti_3C_2T_x$ electrode with 20% carbon (bottom, red), and same electrode after 30 cycles (top, black).

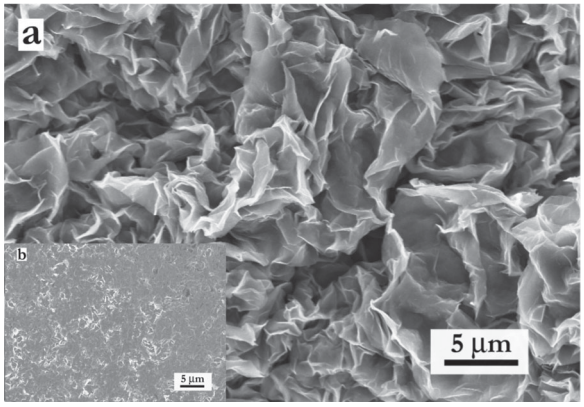

Figure 3. Top view SEM images of (a) *c*-$Ti_3C_2T_x$ flakes, (b) *f*-$Ti_3C_2T_x$ flakes(inset).

presence of a (110) peak at $\sim$ 61° 2θ in the XRD pattern of *c*-$Ti_3C_2T_x$—and its absence in the XRD pattern of *f*-$Ti_3C_2T_x$, indicates that flakes in the *f*-$Ti_3C_2T_x$ films are more ordered parallel to the substrate than the *c*-$Ti_3C_2T_x$ flakes [20–22]. The d-spacings—taken to be half of the c lattice parameter, $d_{c/2}$—of $\sim$13–14 Å for, both *c*-$Ti_3C_2T_x$ and *f*-$Ti_3C_2T_x$, were calculated from the position of (002) peak. These values are significantly higher than the $d_{c/2}$ (9.7 Å) calculated for ML $Ti_3C_2T_x$ powders [13]. The XRD pattern of the electrodes containing *c*-$Ti_3C_2T_x$, carbon black and the polyvinylidene fluoride (PVDF) binder (Figure 2(b)) reveals the absence of the (110) peak. This somewhat unexpected result can be ascribed to the shearing of the MXene nanosheets during the fabrication of the electrode. This shear could reduce the intensities of the *c*-$Ti_3C_2T_x$ peaks in the XRD pattern diminishing the already weak signal from the (110) atomic planes. Using the Scherrer equation, we find that the *c*-$Ti_3C_2T_x$ powders have aggregates with the thickness of $\sim$16–17 layers of MXene. The aggregate thickness reduces to 8–9 layers in the electrodes.

Top view scanning electron microscopy (SEM) images of *c*-$Ti_3C_2T_x$ powders (Figure 3) and *f*-$Ti_3C_2T_x$ films (inset in Figure 3) reveal that the former comprises a foam-like, 3D interpenetrating porous structure. The microstructure of *f*-$Ti_3C_2T_x$, on the other hand, is typical of filtered MXene films and shows how well the 2D flakes stack on top of each other [16]. Energy-dispersive X-ray spectroscopy, EDs, analysis revealed no appreciable change in chemical composition of *f*-$Ti_3C_2T_x$ and *c*-$Ti_3C_2T_x$ (Supp. Info. Table S1), indicating that enhancement of the electrochemical performance is mainly due to the material's mesoporous crumpled morphology.

The open structure observed in the SEM images was further investigated by N_2 absorption/desorption (Supp. Info. Fig. S2a). The isotherm shows a type-4 behavior indicating the presence of mesopores. The hysteresis loop further matches with H3-type loops, which corresponds to aggregates of plate like particles with slit pores [23], which is in agreement with the nanosheet morphology. The presence of mesopores is also confirmed by the pore size distribution (Supp. Info. Fig. S2b), where a high concentration of 3–5 nm pores is deduced. The surface area of *c*-$Ti_3C_2T_x$ is 33 $m^2 g^{-1}$ which is comparable to that of multilayer MXenes [24]. For reasons that are not clear, this value is significantly lower than the value of $\approx$105 $m^2 g^{-1}$ reported by Shah et al. [17].

One of this work's basic premises is that the open, porous architecture of the *c*-$Ti_3C_2T_x$ powder should facilitate electrolyte penetration and improve accessibility for Na^+ ions through the electrodes. By now it is reasonably well-established that 'card house' like morphologies of graphitic sheets in hard carbon show higher capacities than graphite in sodium Ion Batteries (NIBs) [25,26]. To demonstrate this idea, we compared the electrochemical characteristics of our *c*-$Ti_3C_2T_x$ powder with filtered films made of the same colloidal suspension (Supp. Info. Fig. S5c).

An SEM image of the electrode (Supp. Info. Fig. S1, the area inside the circle) shows that even though the nanosheets are sheared and the addition of carbon black and PVDF binder, the crumpled flake morphology, with random orientation, is still maintained, confirming that the disappearance of (110) peak from the XRD pattern (Figure 2b) is caused by a diminished intensity of the peaks and not from preferential alignment in the basal planes.

The acid-induced flocculation and crumpling can be understood by considering the interaction between the charged species involved in the process. Colloids based on $Ti_3C_2T_x$ are pH sensitive and below their isoelectric point, the suspension is no longer stable and as a result the flakes crash out of solution [27]. In a colloidal suspension, the MXene nanosheet surfaces are negatively charged due to the presence of the –O, –OH, and –F functional groups. If the electrostatic repulsion between the layers is larger than the Van der Waals attraction the colloid is stable. Upon addition of HCl, the H^+ ions presumably form an electric double layer on the sheets, reducing their negative surface charges, leading to rapid aggregation due to the Van der Waals attraction and eventually complete flocculation. These observations are consistent with the Derjaguin, Landau, Verwey, and Overbeek theory for colloid stability. Similar crashing phenomena have been reported for colloidal suspensions of graphene oxide, kaolinite, and aluminum oxide [28–30].

Cyclic voltammetry was used to probe the intercalation of Na^+ ions into *c*-$Ti_3C_2T_x$ electrodes in a non-aqueous electrolyte. The irreversible anodic peak observed at 0.9 V in the first cycle (Supp. Info Fig. S3a) is

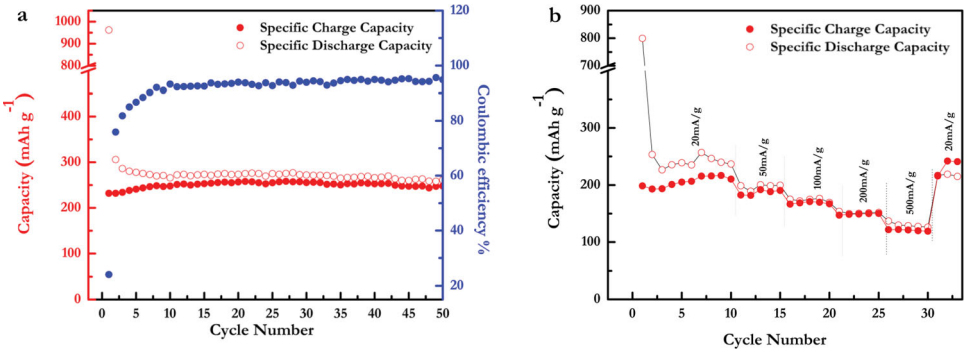

Figure 4. (a) Cycling Electrochemical performance of Na-ion cells containing electrodes made with 70% *c*-$Ti_3C_2T_x$, 20% carbon black, 10 wt.% PVDF: a) cycling stability at current density of 20mA g^{-1} and, (b) Rate performance at currents densities of 20, 50, 100, 200, and 500 mA g^{-1}.

most probably due to the formation of a solid-electrolyte interphase (SEI) layer on the electrode surface. This peak is characteristic of the $Ti_3C_2T_x$ MXene electrodes in Na-ion batteries during first discharge [11,13,16]. The absence of this peak in further cycles indicates that the SEI formed is stable which helps the electrode retain its capacity over many cycles [31].

The anodic and the cathodic peaks around 0.1 V (Supp. Info. Fig. S3a) can be ascribed to the intercalation of Na^+ ions into the carbon black used as the conductive additive. To verify this, we cycled electrodes with, and without, carbon black; in the latter curves, the aforementioned peaks are absent (Supp. Info. Fig. S3b) [32].

We observe that the addition of 20 wt.% carbon to electrodes nearly doubles the capacity of the *c*-$Ti_3C_2T_x$ electrodes and also improves its cycling performance (Supp. Info. Fig. S5a). Even though individual MXene nanosheets are highly conducting, the crumpling appears to lower the overall conductivity, presumably as a result of reduced flake-to-flake overlap [33,34]. The addition of carbon black solves this problem by creating more pathways for electrons transfer. On the down side, the addition of carbon black greatly increased the degree of irreversibility observed in the first cycle again presumably due to the formation of an SEI on the carbon surface [35].

The crumpled MXene electrode exhibited an initial reversible capacity of 250 mAh g^{-1} at a current density of 20 mA g^{-1} (Figure 4(a)), which is one of the highest capacities reported for any MXene phase in Na-ion electrochemical system to date (Supp. Info. Table S2). As shown in Figure 4(a), after the first 10 cycles, the *c*-$Ti_3C_2T_x$ electrode exhibits stable electrochemical performance with capacities in the 10th and 50th cycles of 248 and 246 mAh g^{-1}, respectively. The low Columbic efficiency of the first few cycles is attributed to SEI formation, the irreversible trapping of Na^+ ions in the material, and possibly a reaction between the Na^+ ions in electrolyte with the –O, –OH and –F functional groups present on the surface of MXene nanosheets [36]. The observed gradual increase in Columbic efficiency up to ≈95% after 50 cycles (Figure 4(a)) is consistent with previous reports by Kajiyama et al. and Xie et al. [13,14]. Additionally, Kajiyama et al. have shown that solvent molecules tend to intercalate irreversibly between the MXene layers along with Na^+ ions, hampering the interconnectivity of MXene nanosheets [13]. The 5 Å increase in $d_{c/2}$, after cycling (Figure 2(b)) suggests that a similar phenomenon occurs in the case of our *c*-$Ti_3C_2T_x$ electrodes.

The evaluation of the rate performance of *c*-$Ti_3C_2T_x$ electrodes (Figure 4(b)) revealed that the discharge capacity drops down from 240 mAh g^{-1} at 20 mA g^{-1} to 190 mAh g^{-1} at 50 mA g^{-1}, 170 mAh g^{-1} at 100 mA g^{-1}, 150 mAh g^{-1} at 200 mA g^{-1}, and 120 mAh g^{-1} at 500 mA g^{-1}. When the current is decreased to its initial value of 20 mA g^{-1}, the specific capacity returns to 240 mA g^{-1}.

It is important to note that when the process was repeated with nitric or sulfuric acid, the same crumpling phenomenon was observed. Whether the latter powders are different from the ones obtained herein is beyond the scope of this work but should be investigated in more detail. Acetic acid (CH_3COOH) or propionic acid (C_2H_5COOH), on the other hand, does not work. It is also important to point out that similar to Shah et al. [17], who created crumpled $Ti_3C_2T_x$ by spray drying, the crumpling can be reversed by placing the powders in neutral water.

Lastly, in a companion paper, that has been submitted for publication, we showed that by simply increasing the pH of a $Ti_3C_2T_x$ colloidal suspension using common alkali metal hydroxides, crumpled flakes, quite similar to the ones observed here, are formed.

Conclusions

Herein, we show that simply reducing the pH—of a near-neutral colloidal $Ti_3C_2T_x$ suspension—results in the crashing out of the 2D nanosheets. The resulting powders are crumpled and create a 3D mesoporous open architecture. Notably, the latter is achieved without additives or spacers, such as CNTs, graphene sheets and/or complicated templates. This method is simple, inexpensive, imminently scalable and probably applies to most MXenes. Electrodes made with the crumpled powders, together with carbon black and a binder, showed quite promising results in Na-ion batteries.

Acknowledgements

The authors thank Pieralberto Collini and Kinjal Valendra for their aid with MXene synthesis, Justin Li helping with the SEM. Tyler Mathis for helping with BET and, Sankalp Kota and Bryan Byles for useful discussions.

Disclosure statement

No potential conflict of interest was reported by the authors.

Funding

This work was funded by the Swedish Research Council (Project Grant No. 621-2014-4890). EP and MC thank the support from the National Science Foundation, Division of Materials Research (Grant No. DMR-1609272).

ORCID

Michel W. Barsoum http://orcid.org/0000-0001-7800-3517

References

[1] Naguib M, Kurtoglu M, Presser V, et al. Two-Dimensional nanocrystals produced by exfoliation of Ti_3AlC_2. Adv Mater. 2011;23:4248–4253.
[2] Naguib M, Mashtalir O, Carle J, et al. Two-Dimensional transition metal carbides. ACS Nano. 2012;6:1322–1331.
[3] Zhang X, Zhang Z, Zhou Z. MXene-based materials for electrochemical energy storage. J Energy Chem. 2018;27:73–85.
[4] Zhang Q, Teng J, Zou G, et al. Efficient phosphate sequestration for water purification by unique sandwich-like MXene/magnetic iron oxide nanocomposites. Nanoscale. 2016;8:7085–7093.
[5] Liu Y, Du H, Zhang X, et al. Superior catalytic activity derived from a two-dimensional Ti_3C_2 precursor towards the hydrogen storage reaction of magnesium hydride. Chem Commun. 2016;52:705–708.
[6] Li R, Zhang L, Shi L, et al. MXene Ti_3C_2: An effective 2D light-to-heat conversion material. ACS Nano. 2017;11:3752–3759.
[7] Han M, Yin X, Wu H, et al. Ti_3C_2 MXenes with modified surface for high-performance electromagnetic absorption and shielding in the X-band. ACS Appl Mater Interfaces. 2016;8:21011–21019.
[8] Mashtalir O, Naguib M, Dyatkin B, et al. Kinetics of aluminum extraction from Ti_3AlC_2 in hydrofluoric acid. Mater Chem Phys. 2013;139:147–152.
[9] Barsoum MW. The $M_{N+1}AX_N$ phases: a new class of solids. Prog Solid State Chem. 2000;28:201–281.
[10] Er D, Li J, Naguib M, et al. Ti_3C_2 MXene as a high capacity electrode material for metal (Li, Na, K, Ca) Ion batteries. ACS Appl Mater Interfaces. 2014;6:11173–11179.
[11] Xie Y, Dall'Agnese Y, Naguib M, et al. Prediction and characterization of MXene nanosheet anodes for non-lithium-Ion batteries. ACS Nano. 2014;8:9606–9615.
[12] Yu Y-X. Prediction of mobility, enhanced storage capacity, and volume change during sodiation on interlayer-expanded functionalized Ti_3C_2 MXene anode materials for sodium-Ion batteries. J Phys Chem C. 2016;120:5288–5296.
[13] Kajiyama S, Szabova L, Sodeyama K, et al. Sodium-ion intercalation mechanism in MXene nanosheets. ACS Nano. 2016;10:3334–3341.
[14] Xie X, Zhao M-Q, Anasori B, et al. Porous heterostructured MXene/carbon nanotube composite paper with high volumetric capacity for sodium-based energy storage devices. Nano Energy. 2016;26:513–523.
[15] Zhao M-Q, Xie X, Ren CE, et al. Hollow MXene spheres and 3D macroporous MXene frameworks for Na-Ion storage. Adv Mater. 2017;29:1702410.
[16] Lian P, Dong Y, Wu Z-S, et al. Alkalized Ti_3C_2 MXene nanoribbons with expanded interlayer spacing for high-capacity sodium and potassium ion batteries. Nano Energy. 2017;40:1–8.
[17] Shah SA, Habib T, Gao H, et al. Template-free 3D titanium carbide ($Ti_3C_2T_x$) MXene particles crumpled by capillary forces. Chem Commun. 2017;53:400–403.
[18] Vaughn A, Ball J, Heil T, et al. Selective calixarene-directed synthesis of MXene plates, crumpled sheets, spheres, and scrolls. Chem A Eur J. 2017;23:8128–8133.
[19] Du F, Tang H, Pan L, et al. Environmental friendly scalable production of colloidal 2D titanium carbonitride MXene with minimized nanosheets restacking for excellent cycle life lithium-ion batteries. Electrochim Acta. 2017;235:690–699.
[20] Ghidiu M, Barsoum MW. The {110} reflection in X-ray diffraction of MXene films: misinterpretation and measurement via non-standard orientation. J Am Ceram Soc. 2017;100:5395–5399.
[21] Okamoto H, Kumai Y, Sugiyama Y, et al. Silicon nanosheets and their self-assembled regular stacking structure. J Am Chem Soc. 2010;132:2710–2718.
[22] Ali MA, Tchalala MR. Chemical synthesis of silicon nanosheets from layered calcium disilicide. J Phys Conf Ser. 2014;491:012009.
[23] Thommes M, Kaneko K, Neimark AV, et al. Physisorption of gases, with special reference to the evaluation of surface area and pore size distribution (IUPAC technical report). Pure Appl Chem. 2015;87:113–1069.
[24] Ren CE, Zhao MQ, Makaryan T, et al. Porous two-dimensional transition metal carbide (MXene) flakes for high-performance Li-Ion storage. ChemElectroChem. 2016;3:689–693.
[25] Suryawanshi A, Mhamane D, Nagane S, et al. Indanthrone derived disordered graphitic carbon as promising

insertion anode for sodium ion battery with long cycle life. Electrochim Acta. 2014;146:218–223.
[26] Palomares V, Serras P, Villaluenga I, et al. Na-ion batteries, recent advances and present challenges to become low cost energy storage systems. Energy Environ Sci. 2012;5:5884–5901.
[27] Ying Y, Liu Y, Wang X, et al. Two-Dimensional titanium carbide for efficiently reductive removal of highly toxic chromium(VI) from water. ACS Appl Mater. Interfaces. 2015;7:1795–1803.
[28] Chowdhury I, Mansukhani ND, Guiney LM, et al. Aggregation and stability of reduced graphene oxide: complex roles of divalent cations, pH, and natural organic matter. Environ Sci Technol. 2015;49:10886–10893.
[29] Mui J, Ngo J, Kim B. Aggregation and colloidal stability of commercially available Al_2O_3 nanoparticles in aqueous environments. Nanomaterials. 2016;6:90.
[30] Schofield RK, Samson HR. Flocculation of kaolinite due to the attraction of oppositely charged crystal faces. Discuss Faraday Soc. 1954;18:135–145.
[31] Come J, Naguib M, Rozier P, et al. A non-aqueous asymmetric cell with a Ti_2C-based Two-dimensional negative electrode. J Electrochem Soc. 2012;159:A1368–A1373.
[32] Simon P, Gogotsi Y, Dunn B. Where. Do Batteries End and Supercapacitors Begin? Science. 2014;343:1210–1211.
[33] Ghidiu M, Lukatskaya MR, Zhao M-Q, et al. Conductive two-dimensional titanium carbide "clay" with high volumetric capacitance. Nature. 2014;516:78–81.
[34] Ying G, Dillon AD, Fafarman AT, et al. Transparent, conductive solution processed spincast 2D Ti_2CT_x (MXene) films. Mater Res Lett. 2017;5:391–398.
[35] Alcántara R, Jiménez-Mateos JM, Lavela P, et al. Carbon black: a promising electrode material for sodium-ion batteries. Electrochem Commun. 2001;3:639–642.
[36] Wang X, Kajiyama S, Iinuma H, et al. Pseudocapacitance of MXene nanosheets for high-power sodium-ion hybrid capacitors. Nat Commun. 2015;6:1539.